Cadmium distribution in Pb-Zn slags from Upper Silesia, Poland: implications for cadmium mobility from slag phases to the environment

Tyszka R.[1], Pietranik A.[*2], Kierczak J.[2], Zieliński G.[3], Darling J.[4]

[*] corresponding author: Anna Pietranik, University of Wrocław, Institute of Geological Sciences, Borna 9, 50-204, Wrocław, Poland, anna.pietranik@uwr.edu.pl

[1]Wroclaw University of Environmental and Life Sciences, Institute of Soil Science and Environmental Protection, C.K.Norwida 25, 50-375 Wrocław Poland, tyszka.rafal@gmail.com
[2]University of Wroclaw, Institute of Geological Sciences, Borna 9, 50-204, Wroclaw, Poland, jakub.kierczak@uwr.edu.pl
[3]Polish Geological Institute, Rakowiecka 4, 00-975, Warsaw, Poland, gzie@pgi.gov.pl
[4]University of Portsmouth, School of Earth and Environmental Sciences, University House Winston Churchill Avenue PO1 2UP, Portsmouth, UK, james.darling@port.ac.uk

HIGHLIGHTS

1. Cadmium-rich slag offers insight into Cd distribution and potential mobility
2. Cd is strongly incompatible and enriched only in late melts and not major phases
3. Most of the Cd budget is limited to 5-10 μm Pb silicates
4. Cd can be easily accessed during weathering of slag
5. Cd behaviour is different to that of other PTE

ABSTRACT

Cadmium is a toxic element, generally highly mobile and easily transferred from Cd-bearing ore minerals to the environment as shown by numerous leaching experiments and studies of biota. However, the behaviour of Cd is less understood during smelting activities, when it is transferred from Cd-bearing ore to the metal as well as to the smelting by-product - slag. Slag material, with Cd concentrations over 500 mg/kg, occurs at an abandoned slag pile after Pb-Zn metal smelting in Swiętochłowice (Upper Silesia). Such material, extremely enriched in Cd (15 mg/kg is a legislative guideline for industrial soils), offers a possibility to study the distribution of Cd within slag fragments composed of silicates and oxides, gaining insight into Cd mobility. Electron microprobe analyses of primary slag show that Cd partitioning between different phases is not controlled by site preference and Cd does not substitute for elements with similar radius, such as Zn in Zn-spinel or Ca in Pb-hardystonite. Cadmium is strongly incompatible and enriched in late melts that, in the case of the studied slag, crystallize Pb-

hardystonite rims, late Pb-silicates, probably alamosite and phosphates. These phases contain most of the Cd budget, but in a small volume (5-10μm phases). As such, Cd behaviour and distribution in silicate slags may contrast that of other potentially toxic elements, which are generally selectively partitioned into one or more major phases. The study of another slag fragment, composed of secondary Fe-(hydro)oxides, formed after sulphide weathering, shows low Cd contents suggesting that either Cd was mobilized from the sulphide during weathering or lost in the smelting process. General distribution of Cd within slag in easily accessible parts (enrichment at rims and in late phases occurring at grain boundaries) and not in secondary phases, suggests that Cd have a high potential mobility from the slag to the environment.

KEYWORDS: Pb-Zn slag; Cd partitioning; Cd-rich phases; slag-melt crystallization; slag weathering

1. INTRODUCTION

Cadmium (Cd) is an element, which is not essential for terrestrial plant or animal life or for biological functions in humans and is considered as one of the most toxic elements (Satarug et al., 2003; Patrick, 2003; Witeska et al., 2014; Lane et al. 2015). Cadmium toxicity may be manifested as lung damage, renal dysfunction, hepatic injury, bone defects, hypertension, reproductive toxicity, and teratogenicity (Satarug et al., 2003; Patrick, 2003). Major natural Cd carriers are Zn-Fe sulphides and carbonates (Schwartz, 2000) and both these sources are prone to weathering and, thus, releasing Cd to the environment. Cadmium is also released from smelting by-products, which is consistent with high Cd concentrations in soils, sediments and waters affected by smelting activities (Li and Thornton, 2001; Audry et al.,

2010; Piatak and Seal, 2010; Ettler et al., 2012). Cadmium enriched soils are of particular significance since the majority of Cd intake by humans and animals is via eating food grown in Cd-contaminated soil. If Cd is present in soils affected by smelting, it is generally highly bioavailable and tends to bioaccumulate, especially in low pH, oxidized conditions with low organic matter content, large soil particle sizes and high soil moisture (Cornu et al., 2007; Godet et al., 2011; Ettler, 2016). On a regional scale, major sources of Cd in soils include atmospheric deposition and direct additions, e.g. fertilizers (Pan et al., 2010). The highest risk of Cd exposure is in the vicinity of industrial plants, especially nonferrous metal extraction facilities, which are often surrounded by abandoned slag heaps similar to the site in the present study (see also Chrastny et al., 2012).

Cadmium is easily released from geogenic sources by oxidation of sulphides and dissolution of carbonates. Subsequently mobilized Cd can precipitate in Cd-rich secondary phases e.g. carbonates and sulphosalts (Schwartz, 2000; Cabala and Teper, 2007). However, a less understood step of Cd transfer in ore-processing is the formation of Cd enriched phases during smelting of Cd enriched sulphides. Non-ferrous metal smelting produces large quantities of solid by-products known as slag (Piatak et al., 2015; Potysz et al., 2015). Slag may contain up to several hundred to thousands mg/kg of Cd (Parsons et al., 2001; Ettler et al., 2009), such is the case in the studied slag heap after Pb-Zn ore smelting in Swietochlowice (up to 100 mg/kg, Puziewicz et al., 2007). Soils and water surrounding slag heaps also may have high Cd concentrations, often exceeding values recommended by legislative regulators, suggesting mobility of Cd from slag to the environment. (e.g. Audry et al., 2004; Cabala and Teper, 2007; Douay et al., 2008; Piatak and Seal, 2010; Ettler, 2016). The same is implied by leaching experiments from both slags and soils surrounding slag heaps showing that Cd is mobile and bioavailable (Chrastny et al., 2012; Ettler et al., 2012).

High Cd mobility from primary slag to secondary phases was also confirmed for the Świetochlowice site, since fine fractions (<50 micrometres), composed predominately of secondary minerals, were consistently enriched in Cd, compared to larger fractions, in which primary minerals were more abundant (Tyszka et al., 2014). However, despite general knowledge on high mobility of Cd, not much is known about its distribution between the slag phases and within slag fragments or a single phase. Cadmium is rarely analysed in situ due to its low concentrations. In this study, two types of slag were examined: "Cd-rich slag" containing silicates and spinels that could be analyzed with high resolution by electron microprobe and "Cd-poor slag" that contained silicates and Fe-(hydro)oxides formed after Zn sulphides weathering. As such, the "Cd-rich slag" provides an insight into Cd distribution and potential mobility, which, we believe, can be extrapolated onto slags with similar mineralogy, but with lower Cd contents. It is because Cd should behave in a similar way in silicate slags composed of spinels and melilite, i.e. common slag phases. On the other hand, "Cd-poor slag" offers insight into Cd mobility from Zn sulphide (major geogenic Cd carrier) to secondary products.

2. ŚWIĘTOCHŁOWICE – SITE DESCRIPTION

The slag heap in Świętochłowice consisted of chemically and mineralogically diverse slags from over a century of Zn-Pb smelting in the nearby "Silesia" plant. The slag heap was composed of several slag types related to changing smelting conditions and ore sources (Puziewicz et al., 2007). The smelting involved predominately Zn-Pb ore from Lower Poland (Trzebinia and Olkusz mines), but sporadically foreign ores were being smelted in the second half of the 20th century (Puziewicz et al., 2007). The smelting factory "Silesia" operated from the middle of 19th century and was closed down in 1974. In 19th and, at the beginning of

20th century, it was the largest Zn smelter in Europe (Barciak, 1999). The smelter activity left the slag heap covering 15ha and up to 25 meters high, the top of the slag heap was flat, which facilitated water infiltration into the heap (Brill et al., 2008).

In recent years the slag was removed and used for undefined construction materials. The slag removal uncovered the interior of the heap, which is composed of strongly weathered reddish, fine-grained material containing larger slag fragments, covered by thick layers of secondary minerals (Tyszka et al., 2014). Unweathered or slightly weathered slags occur only at the surface of the slag heap (Bril et al., 2008; Tyszka et al., 2014). Specifically, two types of the heap remnants occur and they can be observed in vertical profiles: (1) weathered slag interior, covered by clay-rich layer and soil-like material. The clay-rich layer was probably added during remediation attempt as suggested by different heavy minerals assemblages in the layer, compared to those in the slag heap (Tyszka et al., 2016) and (2) weathered slag interior on which natural soil is developed and the remediation layer is absent (Tyszka et al., 2014). Tyszka et al. (2014) suggested that special conditions such as pH variations from acidic to basic may cause extensive weathering within the interiors of slag heaps and produce secondary minerals rich in potentially toxic elements (PTE), which may remain in the semi-stable state.

Cadmium concentrations in whole samples (as analysed in Tyszka et al., 2014) were from 4 to 570 mg/kg and were dependent on the location of the sampled profile, e.g. all samples collected at Site 1 (Fig. 1) were rich in Cd, from over 100 mg/kg to 570 mg/kg. Moreover, the fine fraction (<50 micrometers) was further enriched in Cd with a maximum concentration of 780 mg/kg. In contrast, samples from Site 3 had generally lower Cd concentrations from 4 to 65 mg/kg (Tyszka et al., 2014). Unweathered slag analysed for both Sites 1 and 3 had much

lower Cd concentrations from 0.4 to 1.3 mg/kg, however, the concentrations of Cd reported by Puziewicz et al. (2007) were higher for samples of unweathered slag from Świętochłowice and ranged from 1 to 98 mg/kg. The EDTA leachable concentrations, which represent the easily mobilized fraction, were relatively low for all the weathered slag samples and varied from 3 to 24 % of the whole Cd budget. Also, the proportions were similar between Sites 1 and 3 (Tyszka et al., 2014).

Fig. 1. Schematic map of the slag heap and corresponding profiles at Site 1 and Site 3 (modified after Tyszka et al. 2014). Sites 1 and 3 represent sampling sites from Tyszka et al. (2014). Cadmium values for whole samples shown in profiles are also from Tyszka et al. (2014). Slag fragments were taken from the samples indicated as the white rectangle in each profile.

Figure info – 2 columns, BW in print, colour online

3. ANALYTICAL METHODS

3.1 Electron microprobe

BSE images, mappings (images of the distribution of selected elements in selected areas) and in-situ quantitative chemical analysis were collected using a CAMECA SX-100 electron microprobe in the Micro-Area Analysis Laboratory, Polish Geological Institute, Warsaw. BSE images were collected under the following conditions: 15 kV of accelerating voltage, 10 nA beam current, the beam focused. Based on BSE images and data from energy dispersive X-ray spectrometer (EDS), some areas were selected to prepare elemental mappings for distribution of Cd, P, Pb, S (using wavelength dispersive X-ray spectrometers - WDS with

LPET crystals); Zn, Mn (using WDS spectrometers with LLIF crystals); As, Mg (using WDS spectrometers with TAP crystals); Fe, Al, Si, Ca and K (using EDS spectrometer). Maps were made under the following conditions: 15 kV of accelerating voltage, 40 nA beam current, beam focused.

Quantitative in-situ analyses were done under the following electron beam conditions: 15 kV, 10 nA, the beam focused. Analyzed elements with the line measured, diffraction crystal used, and detection limits are shown in Table A (Supplementary Material).

3.2 Laser Ablation – Inductively Coupled Plasma – Mass Spectrometry

Trace elements in zircon were analysed using Laser Ablation-Inductively Coupled Plasma Mass Spectrometer (LA-ICPMS) at the School Of Earth and Environmental Sciences at the University of Portsmouth. Data were normalised to the glass reference material NIST 610 (Pearce et al., 1997). Complete analyses are presented in Supplementary Material (Table D). Every 18 analyses of unknowns were bracketed by two analyses of NIST 610. Glass NIST 614 was also analysed as an unknown, yielding results in good agreement with the expected values for PTE (Table 1), although many elements were below the detection limit for this standard. The repetitive analyses (n=3) of the NIST 614 standard for those elements which have a concentration above 2 mg/kg yielded accuracy between -10 and 14 % and precision from 2 to 18 % (Table D).

Data were reduced using software SILLS and with Al analyses from electron microprobe as an internal standard for the Cd-poor sample and Zn and Mg concentrations for the Cd-rich sample. The absolute concentrations in mg/kg should be treated with caution as the analysed material was usually heterogeneous and it was difficult to attribute a single Al, Mg or Zn concentration to a single laser spot of 55 micrometre. The chemical variability was

often observed in horizontal (in microprobe) and vertical directions (in LA-ICPMS). Aluminum was chosen as an internal standard in Cd-poor slag because it showed the least variation between different spots of silicate -minerals (less than 10 %) and an average value of 15 % was attributed to all silicate analyses. Similarly, in the Cd-rich sample, Zn showed the least variability for Zn spinel (27.8 $\pm$ 0.7 wt %, n=15) and the Mg concentration was the least variable in Pb-hardystonite (1.36 $\pm$ 0.15 wt %, n=25). Fe-(hydro)oxides in the Cd-poor sample were more difficult to reduce because all the elements were strongly variable, as is also evident from their compositional mapping by electron microprobe. Ultimately, Al content was also used and the counting times were compared to the counting times of silicates and standards and the Al concentration in unknown was approximated from these observations e.g. if the counting times on Al were identical between standard analysed as unknown and the oxide, the standard concentration of 2 wt % was taken for the reduction. Despite the problems, the reduced concentrations of Zn and Pb in Fe-(hydro)oxides are in good agreement with microprobe data (Table 1) and therefore, we think that the concentrations, even if not perfectly accurate are a good approximation.

4. RESULTS

4.1 Sample choice

Two samples were analysed in detail, taken from the profiles sampled by Tyszka et al. (2014). The first sample “Cd-rich slag” was a slag fragment separated from the sample PS06 of Tyszka et al. (2014) at Site 1, which contained over 500 mg/kg Cd (Figure 1). The second sample “Cd-poor slag” was collected from sample PS20 of Tyszka et al. (op cit.) at Site 3, which contained 34 mg/kg Cd.

It is difficult to constrain how extensive the occurrences of Cd-rich and Cd-poor slag were, so far elevated Cd contents were found in two profiles (Site 1 and unpublished data). However, we do not focus only on the importance of the Cd-rich slag as the major Cd carrier in the heap. Rather, we use the possibility to study this extremely enriched in Cd sample, because it offers a chance to measure Cd contents above detection limits by both microprobe and LA-ICPMS and similar measurements are not possible for slags with lower Cd contents. Also, it consists of the phases typically found as major constituents of Pb-Zn slags i.e. spinel and melilite (Puziewicz et al 2007, Ettler et al. 2009, Piatak and Seal 2010, Warchulski et al 2015). Therefore, we believe that similar processes of Cd enrichment have place also in other slag fragments, where spinel and Pb-Ca-silicates are the major slag phases. On the other hand, the Cd-poor slag sample taken from Site 3 is the typical slag composed of Fe-(hydro)oxides and silicate glass, where Fe-(hydro)oxides replace primary sulphide-rich matte (see below). As such, it represents a sample where Cd was probably initially contained by sulphide minerals – a major natural Cd carrier -and, therefore, may record a common Cd mobilization process happening in situ. In that aspect, we present the two samples as representative of two possible major processes controlling Cd distribution and mobility in slags: the first where Cd was transferred from the ore to silicate slag and the second where Cd was possibly present in sulphide, which was replaced by secondary phases.

4.2 Phases in Cd-rich and Cd-poor slags

The Cd-rich slag is predominately composed of Zn spinel ($Zn(Al,Fe)_2O_4$) and Pb hardystonite ($(Ca,Pb)_2ZnSi_2O_7$, Fig. 2, Fig. 3). Minor phases are larsenite ($PbZnSiO_4$), and probably alamosite ($PbSiO_3$) and phosphohedyphane-hedyphane solid solution ($Ca_2Pb_3(PO_4,AsO_4)_3Cl$). Complete datasets on mineral chemistry from the Cd-rich and Cd-poor samples are included

in Supplementary Material (Table A presents a summary of phases and mineral formula calculations for each slag and Table B and Table C present analyses and corresponding Back Scattered Electron (BSE) images for Cd-rich and Cd-poor slag respectively).

Zn-spinel often occurs as euhedral grains (up to 100 µm) within larger (up to 1 mm) hardystonite (Fig. 3), but may also form individual grains (Fig. 2). It is the first crystallized phase and has variable, negatively correlated Al and Fe concentrations and constant Zn contents approximately 28 wt %. Majority of spinel is a solid solution between gahnite and franklinite with total Fe as Fe_2O_3 (calculated by charge balance, Table A in Supplementary Material). Similar spinel composition was analysed in Świętochłowice slag, assemblage 1 (Puziewicz et al., 2007). Spinel contains Cd-rich inclusions of Pb silicate, probably alamosite. Hardystonite crystallized as the second major phase. It has variable Ca, Zn and Pb concentrations with Pb being negatively correlated with Ca (R^2 = 0.97). Zn varies from 12.0 to 17.7 wt % and Pb from 2.7 to 40.7 wt % (Table 1). Domains of hardystonite with higher Pb concentrations occur at rims (Fig. 2) or as rectangular-like patches one in another (Fig. 3). Phosphates and larsenite form separate phases enclosed in hardystonite (Fig. 3). Phosphates are not ideally recalculated to formula units, which may indicate their mixing with other phases. Larsenite and Pb-rich hardystonite occur also in a form of rounded aggregate enclosed in hardystonite with lower Pb content (Fig. 3).

The Cd-poor slag is composed of silicates with various Si, Ca, Mg and K concentrations and also compositionally heterogeneous Fe-(hydro)oxides (Fig 4, Table C in Supplementary Material). The slag fragment contains variably sized vesicles. The BSE images of Cd-poor slag show brighter and darker phases with clear contours, which we interpret as sub-micrometre crystals and glass (Table C). This is consistent with the chemical variability of the silicate

phase, which may suggest that it is partly crystalline, but the size of crystals is smaller than microprobe resolution. The silicate phase also contains from 0.1 to 1.5 wt % Zn and rarely detectable Pb of up to 0.7 wt % (Table 1). The highest Pb concentrations were noted at the border of the vesicles.

High totals in Fe-(hydro)oxides analyses suggests that majority of the phase is hematite (Fe_2O_3). However, detailed SEM and microprobe survey showed that Fe-(hydro)oxides are composed of numerous small phases including apart from hematite, Fe-(hydro)oxides and inclusions of Pb-rich and Zn-rich oxide phases. The form of Fe-(hydro)oxides is irregular or circular suggesting that it is secondary phase replacing primary minerals or filling empty spaces in glassy, porous slag. The irregular form of Fe-(hydro)oxides suggests that the original contact was that of silicate and sulphide melt and, therefore, the oxides replace primary sulphides. The secondary nature of Fe-(hydro)oxides is evident as the phase fills also late cracks in the slag (Fig. 4).

Fig. 2 Back-scattered electron image and elemental mappings by electron microprobe of Cd-rich slag. The slag fragments with the highest Cd content are marked and accompanied by WDS measurements of Cd concentration. The false colour scale shows relative enrichment in the analyzed element: the black areas contain the minimum elemental concentration and the concentration increases with the colour change from blue, through green, yellow, orange and to red (which always marks the phases with the highest concentration in the analysed BSE image).

Figure info – 2 columns, BW in print, colour online

Fig. 3 Back-scattered electron image and elemental mappings by electron microprobe of Cd-rich slag. Pb hardystonite zone marks hardystonite with approximate formula $(Ca,Pb)_2ZnSi_2O_7$, whereas Pb-hardystonite phases lighter in the BSE images, e.g. those indicated by arrows are closer to the formula $Pb_2ZnSi_2O_7$. The slag fragments with the highest Cd content are marked and accompanied by WDS measurements of Cd concentration. False colour scale as in Figure 2.

Figure info – 2 columns, BW in print, colour online

Fig. 4 Back-scattered electron image and elemental mappings by electron microprobe of Cd-poor slag. False colour scale as in Figure 2.

Figure info – 2 columns, BW in print, colour online

4.2 Distribution of Cd and other potentially toxic elements within the slag samples

Cadmium presence in the Cd-rich sample is confirmed by microprobe analyses and microprobe elemental maps. Cd was detected within silicate phases (Fig. 2), both Cd-rich alamosite and Pb hardystonite. Cadmium is enriched only in the peripheral parts of the hardystonite, at the border with Zn spinel (Fig. 2). The highest Cd concentrations are in alamosite, which occurs in lobes going into the spinel and also in small inclusions within the spinel (up to 2.9 wt % CdO). In other parts of slag, Cd was also detected (up to 0.3 wt % Cd) in rectangular to irregular Pb-rich hardystonite and phosphohedyphane-hedyphane patches/inclusions within the Pb hardystonite (Fig. 3). The major compositional difference between the two shown slag fragments (Fig. 2 and Fig. 3) is that slag in Figure 2 is composed

of phases enriched in Pb, Cd and Fe, whereas the slag in Figure 3 has phases enriched in Ba (Supplementary Material, Table A, Figure A1 and A2).

Fig. 5. Metal(oid)s concentrations in phases from Cd-rich (yellow and orange fields) and Cd-poor samples (blue). Note different composition of major phases (hardystonite and spinel shown in yellow) for most elements, but Cd. LA_ICPMS – Laser Ablation Inductively Coupled Plasma Mass Spectrometry, EM – Electron Microprobe.

Figure info – 2 columns, BW in print, colour online

4.3 Cd concentrations by LA-ICPMS

Cadmium was detected in both Zn-spinel and Pb-hardystonite in Cd-rich slag and only in Fe-(hydro)oxides in Cd-poor slag (Fig. 5). Despite large chemical variability and trace element contents between Zn-spinel and Pb-hardystonite, Cd concentrations overlap between both phases, from 60 to 72 mg/kg in Pb-hardystonite and from 24 to 100 mg/kg in Zn-spinel. On the other hand, Fe-(hydro)oxides contain generally less Cd, from 1 to 19 mg/kg, but strongly variable concentrations of other trace metal(oid)s, often overlapping with the concentrations measured in both spinel and hardystonite.

5. DISCUSSION

5.1 *Implications from Cd distribution in Cd-rich slag on Cd mobility*

The major natural carrier of Cd are sulphides: sphalerite and pyrite (Schwartz, 2000) with sphalerite showing a rather limited range of Cd concentrations from 0.2 to 1 wt % (Cook et

al., 2009). Direct weathering of Cd-bearing ore releases Cd to the environment (Liu et al., 2017), where, depending on the conditions, it can precipitate as Cd-bearing carbonates and sulphosalts (Cabala and Teper, 2007) as well as Cd sulphide - greenockite (e.g. Mogessie et al., 2009). However, processing of the Cd-bearing ore may form a slag enriched in Cd, as is the case at the Świętochłowice site (Puziewicz et al., 2007; Tyszka et al., 2014), and the behavior of Cd in silicate melts is not well understood, since no Cd-bearing silicates occur in nature (IMA list of approved mineral species). The Zn-Pb ore that was smelted in the Świętochłowice plant belongs mostly to the Mississippi Valley-type zinc-lead ores, which were mined in the Cracov-Silesia district. The ore was formed by fluids circulating in Triassic dolomite (Sass-Gustkiewicz and Dżułyński, 1998; Heijlen et al., 2003). The ore smelted at the Świętochłowice site was probably similar to that described for the nearby Katowice-Szopienice area, which was composed of over 80% sphalerite plus minor amounts of wurtzite, marcasite, pyrite, anglesite and dolomite (Warchulski et al., 2016). Therefore, the Cd was most probably introduced into slag by smelting of sphalerite, which contained approximately 0.4 wt % of Cd (Schwartz, 2000).

This study shows that Cd distribution in the Cd-rich slag is not straightforward. Electron microprobe analyses show that Cd is enriched above detection limit only in small areas as rims of Pb-hardystonite or inclusions and embayments consisting of late crystallizing alamosite and to lower extent larsenite and phosphates (Fig. 2, Fig. 3). Similar, late Cd enrichment was observed in the interstitial glass, i.e. the latest melt phase, from Cu slag at the Penn Mine in California, USA (Parsons et al., 2001). In this study, the Cd-rich slag is completely crystallized and the phases that crystallize from such late melts are enriched in many PTE that include Cd and Pb. Additionally, Cd is also enriched in rectangular to irregular patches composed of Pb-enriched hardystonite and included in hardystonite with lower Pb

Fig. 6. Mechanisms of Cd distribution in slag phases.

Figure info – 1.5 column,

concentrations (Fig. 3). Interestingly, this structure closely resembles structures formed in minerals during fluid assisted dissolution-reprecipitation experiments (e.g. rectangular melt inclusions in plagioclase in Holtz and Johannes, 1992 or parallel inclusions in reacted regions in apatite, Harlov et al., 2005; Broom-Fendley et al., 2016). This indicates that similar late dissolution of the slag sample, possibly by hot fluids circulating in the slag pile after deposition, could cause further redistribution of Cd and other PTE. Lower Fe concentrations are found in slag formed by such dissolution than in those not affected by the process (Fig. A2), suggesting fluids were oxidizing and Fe was mobilized from reacted parts as Fe(III). Also, enrichment in Ba in reacted hardystonite and larsenite (Fig. A2) are likely related to the composition of circulating fluids.

Cadmium occurs in vastly different phases including alamosite, hardystonite and phosphates (phosphohedyphane-hedyphane) with the implication that Cd is a strongly incompatible element and is not partitioned in any major phase until late crystallization. Additionally, Cd can be enriched in partial melts when they are formed in a still hot slag pile. Altogether Cd-rich phases may be formed in four different processes, presented here in the order of the timing of crystallization in the cooling slag material (Fig. 6): (1) enrichment in rims of major silicates, in this case Pb-hardystonite, (2) crystallization of alamosite in melt inclusions locked in major phases, in this case Zn spinel and hardystonite, (3) crystallization of alamosite in very late melts at the contact between major phases (4) crystallization of Pb-enriched hardystonite and phosphohedyphane-hedyphane from partial melts/fluids, but with generally lower Cd contents than those observed in all of the above processes.

Strong Cd incompatibility is also implied by Cd concentrations measured by LA-ICPMS in Pb-hardystonite and Zn-spinel. In both phases Cd concentrations are overlapping, with Pb-hardystonite (Cd = 66 ± 5 mg/kg, 1σ, n=5) being more homogenous than Zn-spinel (Cd = 65 ± 27 mg/kg, 1σ, n=4). Overlapping in Cd concentrations between these two phases is surprising as they are vastly different in crystal structure and composition. For example, they contain distinct concentrations of both major constituents like Zn and Pb and trace constituents like Co, Cu, As, Sn, Sb and Th, which are higher in spinel, and Ag and Sr, which are higher in hardystonite. In particular, Cd should be compatible in Zn spinel, since it was shown experimentally that the synthetic $ZnFe_2O_4$ and $CdFe_2O_4$ may form continuous solid solution (Otero-Arean et al., 1988). On the other hand, Cd was shown to be slightly compatible to slightly incompatible in Ca phases, as shown by experimental work on natural melts (Adam and Green, 2006). Therefore, Cd is expected to preferentially partition into Zn-spinel compared to Pb-hardystonite. However, Cd seems highly incompatible in both phases at least until late crystallization of hardystonite rims. Also, it does not partition according to the site preference rules. In fact, it is the most enriched in Pb silicate (alamosite), a mineral, which has no structural component, which should be substituted by Cd. Therefore, we suggest that Cd measured by LA-ICPMS is not a constituent of major minerals, but rather a passive component included into the laser analyses due to the incorporation of Cd-rich inclusions mostly composed of alamosite or Pb enriched hardystonite rims. Such inclusions are similar to those analysed by electron microprobe and are not easily separated from major phases during relatively low-resolution laser analyses. Variations in Cd concentration in the spinel phase could be caused by higher abundances of randomly distributed inclusions.

The major implications coming from Cd distribution in the Cd-rich slag is that Cd can be highly enriched in relatively small areas (5-10 μm) and in easily accessible parts of the slag (phase rims and grain boundaries). Therefore, weathering of the slag will preferentially remove Cd-rich parts of the major phases, such as the rims of Pb-hardystonite and embayments filled with alamosite, which constitute the majority of Cd budget in the slag. Also, high incompatibility of Cd causes its enrichment in mineral lattices, where Cd does not substitute for elements similar in size, such as Zn and Ca. It is, therefore, possible that such Cd is more easily released from the lattice than elements, which are more fitted to the sizes of the structural sites.

In this study, we used Cd-rich slag as a representative example of possible Cd distribution in a crystalline slag composed of silicates and oxides. Cadmium distribution can be similar also in slags with lower Cd contents, but with similar phase composition and, therefore, Cd should be generally easily mobilized when the major slag silicates are weathered. On the other hand, Cd may be less mobile in slags dominated by inclusion-rich spinels as spinel is generally a stable phase (Kierczak et al. 2013) and can protect Cd-rich inclusions from weathering.

5.2 Distinct origin of Cd in Cd-rich and Cd-poor slag

Cadmium was not detected by electron microprobe in Cd-poor slag, however, Cd concentrations up to 18 mg/kg were measured in Fe-(hydro)oxides by laser ablation. On the other hand, Cd concentrations in silicates were generally below or sometimes slightly above the detection limit of the laser analyses (up to 2.5 mg/kg). These different concentrations of Cd between Fe-(hydro)oxides and silicates, compared to similar concentrations in the phases

from Cd-rich slag, suggest that different processes controlled Cd distribution in Cd-rich and Cd-poor slags.

The Cd-poor and Cd-rich slag samples had different origins in that Cd-rich slag represented the fully smelted product, whereas Cd-poor slag was a mixture of the sulphide and silicate melts produced during smelting and sulphides were later replaced by secondary phases. Replacement of sulphides by secondary Fe-(hydro)oxides is a process commonly observed in different slag samples (e.g. Lanteigne et al., 2012; Kierczak et al., 2013) and similar origin of Fe-(hydro)oxides is suggested for the Cd-poor slag since (a) the irregular to circular form of Fe-(hydro)oxides is similar to that of sulphides in less weathered slag samples (Kierczak et al., 2013) and (b) remnants of sulphides are still preserved within the sample in places where small sulphide is surrounded by unweathered glass (Field 4_5 in Table C in Supplementary Material). Interestingly, Cd content in this remaining sulphide is below the detection limit of electron microprobe (avg. 850 mg/kg), even though it was formed by melting of original Cd-rich ore (up to 0.4 wt % Cd, Schwartz, 2000). However, sulphides in slags have a variable composition and may be impoverished in metals, which were recovered during the smelting process (Potysz et al., 2016). In fact, the sulphide in the Cd-poor slag is (Zn,Fe)S (rudashevskyite) rather than the original ore component ZnS (sphalerite). Cadmium is recovered during smelting of Zn-Pb ores together with Zn, with approx. 72-92 % recovery (Shiel et al., 2010), therefore sulphide melt should have lower contents of Cd than the original ore. However, the whole material Cd content for the Cd-poor sample (sample PS20, Tyszka et al. 2014), which includes larger slag fragments and fine-grained material rich in hematite, gypsum and other secondary phases is over 34 mg/kg (Fig. 1, Tyszka et al. 2014). It is almost twice higher than the highest value measured in Fe-(hydro)oxide, which is consistent with Cd being mobilized during weathering and formation of secondary Fe-

(hydro)oxide phases. Therefore, we suggest that Cd, currently present in the Fe-(hydro)oxides, was initially a constituent of primary sulphides and some of Cd remained *in situ* after their decomposition and some was mobilized and presently resides in secondary minerals in the slag heap. Because Cd concentration in sulphide is not known, It is difficult to estimate (1) how much Cd was mobilized in the weathering process, (2) how much of it remained in unknown secondary phases in the heap and (3) how much was mobilized outside the heap. The presence of Fe-(hydro)oxides in cracks (Fig. 4) suggests high mobility of secondary fluids, which were a potential carrier of Cd.

Therefore, the general conclusion is that the origin of Cd and the processes controlling Cd distribution can vary within a slag heap after Pb-Zn metal smelting. However, regardless the Cd origin, most of the Cd-rich phases are prone to weathering either because of their composition (replacement of sulphides by Fe-(hydro)oxides), size (high Cd concentrations contained in small areas) or because of their preferential structural position within the slag samples (rims, late phases extremely enriched in Cd). As such, Cd is expected to be easily mobilized from slag piles. The general high Cd mobility from slag to the environment was confirmed by numerous leaching tests on slags with different composition (summarized in Piatak et al., 2015, Fig. 15). For example, Cd in the leachate is between 0.7 to over 14 % of the total Cd concentration in the Hegeler Zn slag, whereas other minor elements such as Pb and Cu are generally below 0.5 % (Piatak and Seal, 2010). Similar to Cd, significant amounts of Zn are leached (0.1 to 31 %), however, this element is a major constituent of several slag phases, some of which are weather more easily than others (Piatak and Seal, 2010).

6. CONCLUSIONS

Analyses of Cd-rich and Cd-poor slag from the weathered zone in slag heap after Pb-Zn smelting in Świętochłowice show two origins of Cd in the slag. Cadmium can be either transferred to melt during smelting and crystallize as silicate-oxide slags (as represented by Cd-rich slag) or can remain in Cd-enriched-sulphides and their weathering products (as was the case with Cd-poor slag). In the Cd-rich slag, Cd was distributed among late crystallizing phases such as rims of Pb-hardystonite or Pb silicates and it was strongly incompatible in early crystallizing phases such as Pb hardystonite and Zn-spinel, despite their enrichment in other PTE. As such most of the Cd budget was confined in small phases (5-10 μm) occurring at the boundaries between major phases. Such structural position of Cd-rich phases implies the high potential for Cd mobility. Cadmium could be also redistributed by fluid assisted melting when it was incorporated into phosphates, larsenite and Pb-hardystonite formed from partial melts. On the other hand, our Cd-poor slag was a particular sample, initially enriched in sulphides. In that sample, Cd was detected only in secondary Fe-(hydro)oxides, which were the product of sulphides weathering, probably original Cd carriers. Cadmium was mobilized from this sample in the similar manner as it is mobilized from the original ore minerals.

We suggest that samples analysed in this study could be treated as a test and similar Cd distribution can be expected in other slag samples, which are also composed either of silicates and oxides (as Cd-rich slag) or sulphides/oxides and silicates (as Cd-poor slag) and are less enriched in Cd. However, the general implication is that Cd can be bound to different phases and can be released in different conditions, but most of it is easily accessible during weathering.

ACKNOWLEDGEMENTS

The authors would like to thank Nadine Piatak and the anonymous reviewer as well as the editor Robert Ayuso for valuable comments that improved the final version of the manuscript. This work is funded by the National Science Centre in Poland (project OPUS No. UMO-2014/13/B/ST10/01120 to Rafal Tyszka).

Table and Figure captions

Table 1

Comparison of Laser Ablation ICPMS and Electron Microprobe data for analysed slag phases and comparison of analysed and certified values for NIST614 glass (after www-s.nist.gov).

Figure captions

Fig. 1 Schematic map of the slag heap and corresponding profiles at Site 1 and Site 3 (modified after Tyszka et al. 2014). Site 1 and 3 represent sampling sites from Tyszka et al. (2014). Cd values for whole samples shown in profiles are also from Tyszka et al. (2014). Slag fragments were taken from the samples indicated in each profile.

Fig. 2 Back-scattered electron image and elemental mappings by electron microprobe of Cd-rich slag. The slag fragments with the highest Cd content are marked and accompanied by WDS measurements of Cd concentration. The false colour scale shows relative enrichment in the analyzed element: the black areas contain the minimum elemental concentration and the concentration increases with the colour change from blue, through green, yellow, orange and to red (which always marks the phases with the highest concentration in the analysed BSE image).

Fig. 3 Back-scattered electron image and elemental mappings by electron microprobe of Cd-rich slag. Pb hardystonite zone marks hardystonite with approximate formula $(Ca,Pb)_2ZnSi_2O_7$, whereas Pb-hardystonite phases lighter in the BSE images, e.g. those indicated by arrows are closer to the formula $Pb_2ZnSi_2O_7$. The slag fragments with the highest Cd content are marked and accompanied by WDS measurements of Cd concentration. False colour scale as in Figure 2.

Fig. 4 Back-scattered electron image and elemental mappings by electron microprobe of Cd-poor slag. False colour scale as in Figure 2.

Fig. 5 Metal(oid)s concentrations in phases from Cd-rich (yellow and orange fields) and Cd-poor samples (blue). Note different composition of major phases (hardystonite and spinel shown in yellow) for most elements, but Cd. LA-ICPMS – Laser Ablation Inductively Coupled Plasma Mass Spectrometry, EM – Electron Microprobe.

Fig. 6 Mechanisms of Cd distribution in slag phases.

REFERENCES

Adam, J., Green, T., 2006. Trace element partitioning between mica- and amphibole-bearing garnet lherzolite and hydrous basanitic melt: 1. Experimental results and the investigation of controls on partitioning behavior. Contrib. Min. Petrol.152, 1-17.

Audry, S., Schäfer, J., Blanc, G., Jouanneau, J.-M., 2004. Fifty-year sedimentary record of heavy metal pollution (Cd, Zn, Cu, Pb) in the Lot River reservoirs (France). Environ. Pollut. 132, 413–426.

Audry, S., Grosbois, C., Bril, H., Schäfer, J., Kierczak, J., Blanc, G., 2010. Post-depositional redistribution of trace metals in reservoir sediments of a mining/smelting-impacted watershed (the Lot River, SW France). Appl. Geochem. 25, 778–794.

Barciak, A., 1999. The history of Świętochłowice town. Rocznik Świętochłowicki, t. I pod red. Z. Kapały. City Museum in Świętochłowicach, Świętochłowice. (in Polish)

Bril, H., Zainoun, K., Puziewicz, J., Courtin-Nomade, A., Vanaecker, M., Bollinger, J.C., 2008. Secondary phases from the alteration of a pile of zinc-smelting slags as indicators of environmental conditions: an example from Świętochłowice, Upper Silesia, Poland. Can. Mineral. 46, 1235-1248.

Broom-Fendley, S., Styles, M.T., Appleton, J.D., Gunn, G., Wall, F., 2016. Evidence for dissolution-reprecipitation of apatite and preferential LREE mobility in carbonatite-derived late-stage hydrothermal processes. Am. Mineral. 101, 596–611.

Cabala, J., Teper, L., 2007. Metalliferous constituents of rhizosphere soils contaminated by Zn–Pb mining in southern Poland. Water Air Soil Poll. 178, 351–362.

Chrastný, V., Vaněk, A., Teper, L., Cabala, J., Procházka, J., Pechar, L., Drahota, P., Penížek, V., Komárek, M., Novák, M., 2012. Geochemical position of Pb, Zn and Cd in soils near the Olkusz

mine/smelter, South Poland: effect of land use, type of contamination and distance from pollution source. Environ. Monit. Assess. 184, 2517–2536.

Cook, N.J., Ciobanu, C.L., Pring, A., Skinner, W., Danyushevsky, L., Shimizu, M., Saini-Eidukat, B., Melcher, F., 2009. Trace and minor elements in sphalerite: a LA-ICP-MS study. Geochim. Cosmochim. Ac. 73, 4761–4791.

Cornu, J.Y., Denaix, L., Schneider, A., Pellerin, S., 2007. Temporal evolution of redox processes and free Cd dynamics in a metal-contaminated soil after rewetting. Chemosphere 70, 306–314.

Douay, F., Pruvot, C., Roussel, H., Ciesielski, H., Fourrier, H., Proix, N., Waterlot, C., 2008. Contamination of urban soils un an area of northern France polluted by dust emissions of two smelters. Water Air Soil Poll. 188, 247–260.

Ettler, V., Johan, Z., Kríbek, B., Šebek, O., Mihaljevič, M., 2009. Mineralogy and environmental stability of slags from the Tsumeb smelter, Namibia. Appl. Geochem. 24, 1–15.

Ettler, V., Mihaljevič, M., Šebek, O., Matys Grygar, T., Klementová, M., 2012. Experimental in situ transformation of Pb smelter fly ash in acidic soils. Environ. Sci. Technol. 46, 10539–10548.

Ettler, V., 2016, Soil contamination near non-ferrous metal smelters: A review. Appl. Geochem. 64, 56–74.

Godet, J. P., Demuynck, S., Waterlot, C., Lemière, S., Souty-Grosset, C., Scheifler, R., Douay, F., Leprêtre, A., Pruvot, C., 2011. Growth and metal accumulation in Porcellio scaber exposed to poplar litter from Cd-, Pb-, and Zn-contaminated sites. Ecotoxicol. Environ. Saf. 74, 451–458.

Harlov, D. E., Wirth, R., Förster, H. J., 2005. An experimental study of dissolution–reprecipitation in fluorapatite: fluid infiltration and the formation of monazite Contrib. Min. Petrol. 150, 268-286.

Heijlen, W., Muchez, P., Banks, D.A., Schneider, J., Kucha, H., Keppens, E., 2003. Carbonate-Hosted Zn-Pb Deposits in upper silesia, Poland: Origin and evolution of mineralizing fluids and constraints on genetic models. Econ Geol 98, 911–932

Holtz, F., Johannes, W., 1992. Melting of plagioclase in granite and related systems: composition of coexisting phases and kinetic observations. Geol. Soc. Spec. Pap. 272, 417-422.

Kierczak, J., Potysz, A., Pietranik, A., Tyszka, R., Modelska, M., Neel, C., Ettler, V., Mihaljevič, M., 2013. Environmental impact of the historical Cu smelting in the Rudawy Janowickie Mountains (south-western Poland). J. Geochem. Explor. 124, 183-194.

Lane, E.A., Canty, M.J., More, S.J., 2015. Cadmium exposure and consequence for the health and productivity of farmed ruminants. Res Vet Sci. 101, 132–139.

Lanteigne, S., Schindler, M., McDonald, A.M., Skeries, K., Abdu, Y., Mantha, N.M., Murayama, M., Hawthorne, F. C., Hochella, Jr. M.F., 2012. Mineralogy and weathering of smelter-derived spherical particles in soils: implications for the mobility of Ni and Cu in the surficial environment. Water Air Soil Poll. 223, 3619–3641.

Li, X.D., Thornton, I., 2001. Chemical partitioning of trace and major elements in soils contaminated by mining and smelting activities. Appl. Geochem. 16, 1693–1706.

Liu, Y.Z., Xiao, T.F., Perkins, R.B., Zhu, J.M., Zhu, Z.J., Xiong, Y., Ning, Z.P., 2017. Geogenic cadmium pollution and potential health risks, with emphasis on black shale. J. Geochem. Explor. 176, 42-49.

Mogessie, A., Bauer, C., De Machuca, B.C., Meissl, E., Bjerg, E., Delpino, S., 2009. Greenockite and associated sulfide mineralization from the Caledonia Group Mines, Blanca Creek, La Huerta Range, San Juan Province, Argentina. Can. Mineral. 47, 129-141.

Otero-Arean, C., Gracia-Diaz, E., Rubio Gonzalez, J.M., Villa Garcia, M.A., 1988. Crystal chemistry of cadmium-zinc ferrites. J. Sol. State Chem. 77, 275-280.

Pan, J., Plant, J.A., Voulvoulis, N., Oates, C.J., Ihlenfeld, C., 2010. Cadmium levels in Europe: implications for human health. Environ. Geochem. Health. 32, 1–12.

Parsons, M.B., Bird, D.K., Einaudi, M.T., Alpers, C.N., 2001. Geochemical and mineralogical controls on trace element release from the Penn Mine base-metal slag dump, California. Appl. Geochem. 16, 1567–1593.

Patrick, L., 2003. Toxic metals and antioxidants: part II, the role of antioxidants in arsenic and cadmium toxicity**.** Altern. Med. Rev., 8, 106–128.

Pearce, N.J.G., Perkins, W.T., Westgate, J.A., Gorton, M.P., Jackson, S.E., Neal, C.R., Chenery, S.P., 1997. A compilation of new and published major and trace element data for NIST SRM 610 and NIST SRM 612 glass reference materials. Geostand. Geoanal. Res. 21, 115–144.

Piatak, N.M., Parsons, M.B., Seal, R.R., 2015. Characteristics and environmental aspects of slag: A review. Appl. Geochem. 75, 236–266.

Piatak, N.M., Seal, R.R., 2010. Mineralogy and the release of trace elements from slag from the Hegeler Zinc smelter, Illinois (USA). Appl. Geochem. 25, 302-320.

Potysz, A., Van Hullebusch, E.D., Kierczak, J., Grybos, M., Lens, P.N.L., Guibaud, G., 2015. Copper Metallurgical Slags - Current Knowledge and Fate: A Review. Crit. Rev. Environ. Sci. Technol. 45, 2424–2488.

Potysz, A., Kierczak, J., Fuchs, Y., Grybos, M., Guibaud, G., Lens, P.N.L., Van Hullebusch, E.D. 2016. Characterization and pH-dependent leaching behaviour of historical and modern copper slags. J. Geochem. Explor. 160, 1-15.

Puziewicz, J., Zainoun, K., Bril, H., 2007. Primary phases in pyrometallurgical slags from a zinc-smelting waste dump, Świętochłowice, Upper Silesia, Poland. Can. Mineral. 45, 1189-1200.

Sass-Gustkiewicz, M., Dżułyński, S., 1998. On the origin of strata-bound Zn-Pb ores in the Upper Silesia, Poland. Ann. Soc. Geol. Pol. 68, 267-278.

Satarug S., Baker J.R., Urbenjapol S., Haswell-Elkins M., Reilly P.E.B., Williams D.J., Moore M.R., 2003, A global perspective on cadmium pollution and toxicity in non-occupationally exposed population**.** Toxicol. Lett. 137, 65–83.

Shiel, A.E., Weis, D., Orians, K.J., 2010. Evaluation of zinc, cadmium and lead isotope fractionation during smelting and refining, Sci. Tot. Env. 408, 2357-2368.

Schwartz, M.O., 2000. Cadmium in Zinc Deposits: Economic Geology of a Polluting Element, Int. Geol. Rev. 42, 445-469.

Tyszka, R., Kierczak, J., Pietranik, A., Ettler, V., Mihaljevič, M., 2014. Extensive weathering of zinc smelting slag in a heap in Upper Silesia (Poland): Potential environmental risks posed by mechanical disturbance of slag deposits. Appl. Geochem. 4,: 70–81.

Tyszka, R., Pietranik, A., Stankowska, S., 2016. Mobility of potentially toxic elements in the Świętochłowice slag heap: evidence from Mineral Liberation Analyzes. 2nd European Mineralogical Conference Abstract Book.

Warchulski, R., Juszczyk P., Gawęda, A., 2016. Geochemistry, petrology and evolutionary computations in the service of archaeology: restoration of the historical smelting process at the Katowice–Szopienice site. Archaeol Anthropol Sci 1-13.

Warchulski, R., Gawęda, A., Kądziołka-Gaweł M., Szopa K., 2015. Composition and element mobilization in pyrometallurgical slags from the Orzeł Biały smelting plant in the Bytom–Piekary Śląskie area, Poland. Mineral. Mag. 79. DOI**:** https://doi.org/10.1180/minmag.2015.079.2.21.

Witeska, M., Sarnowski, P., Ługowska, K, Kowal, E., 2014. The effects of cadmium and copper on embryonic and larval development of ide Leuciscus idus L. Fish. Physiol. Biochem. 40, 151–163.

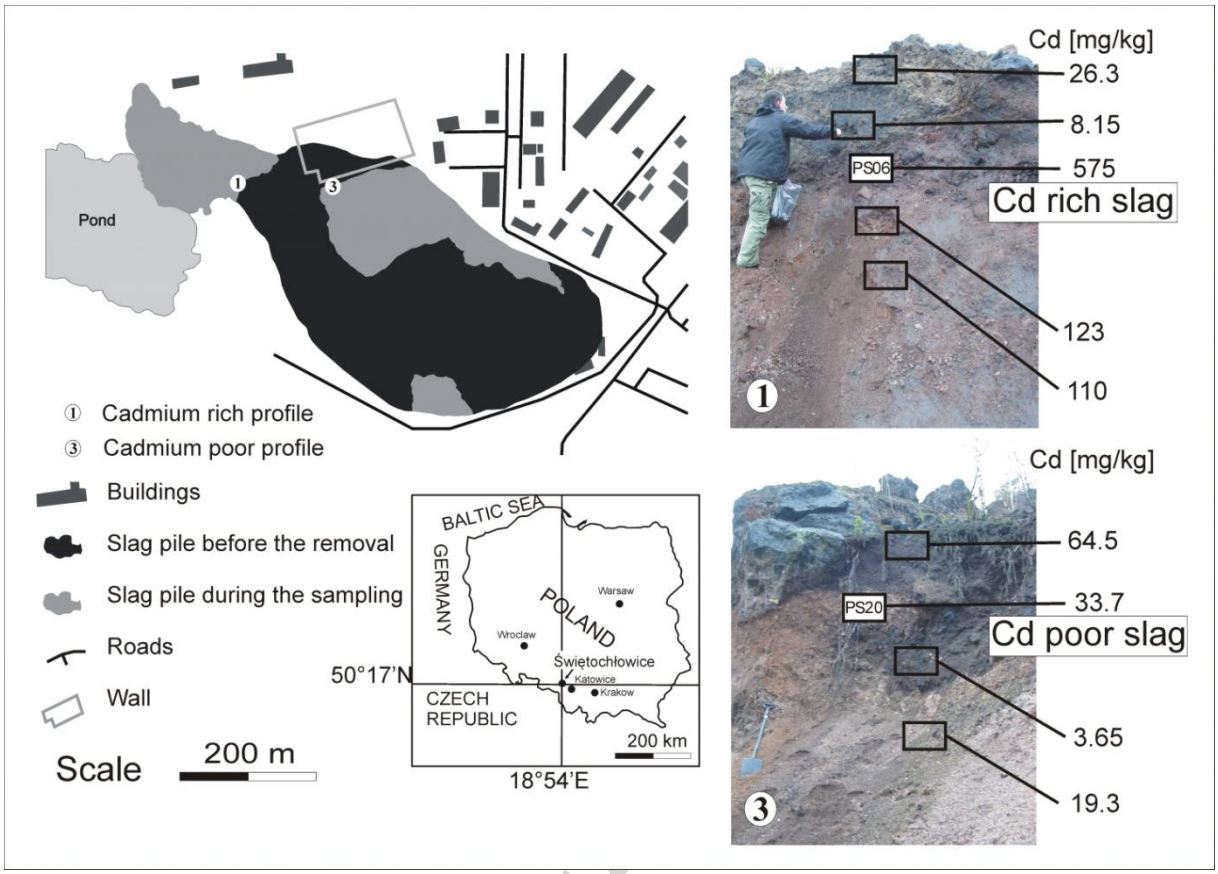

Fig. 1

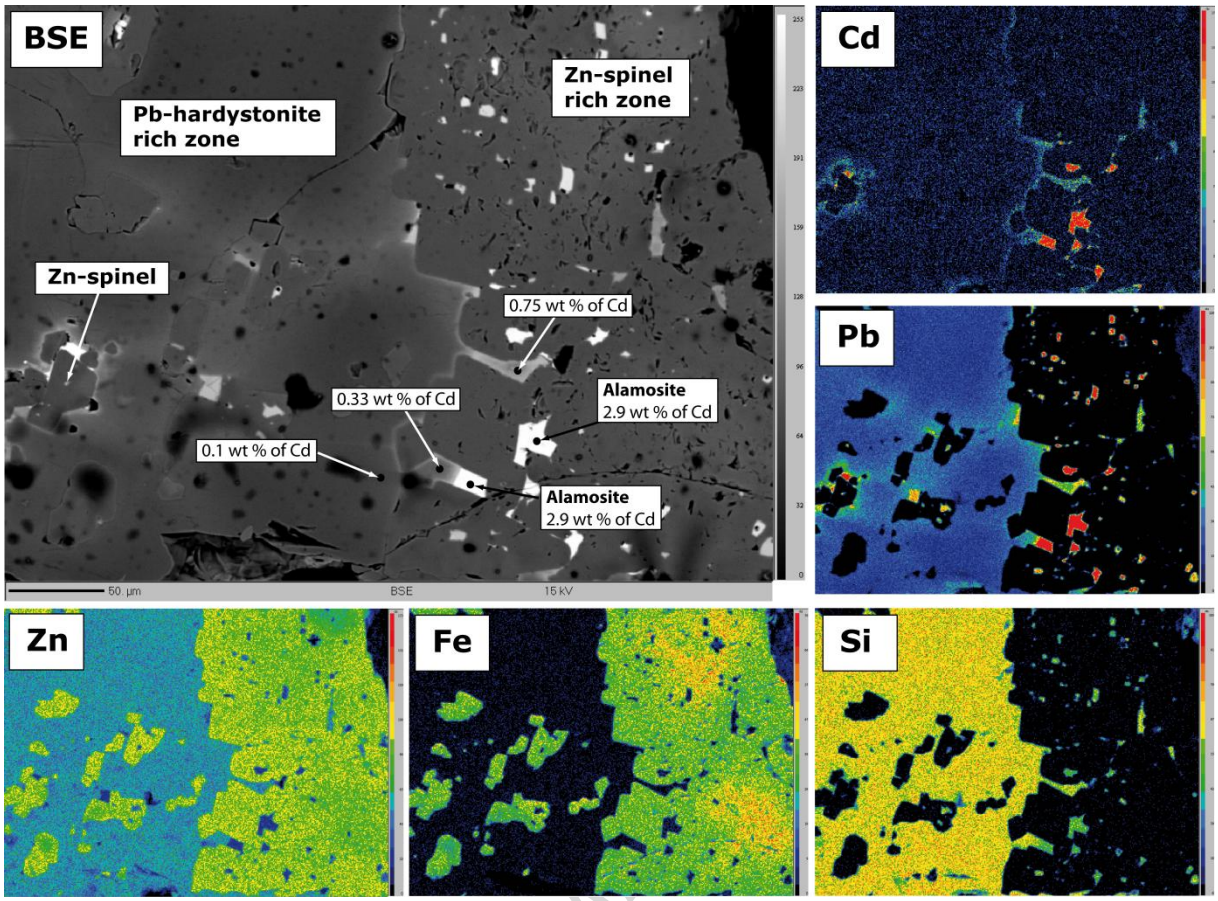

Fig. 2

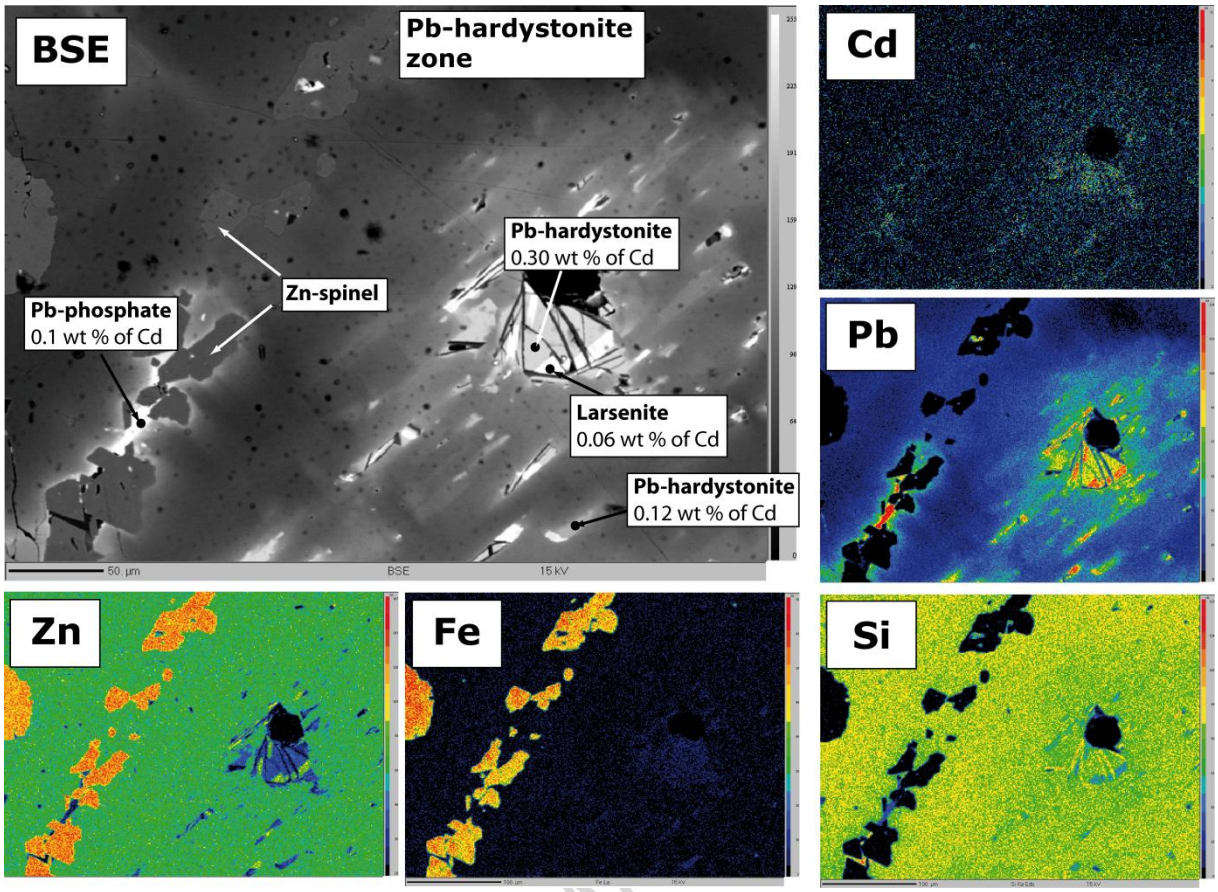

Fig. 3

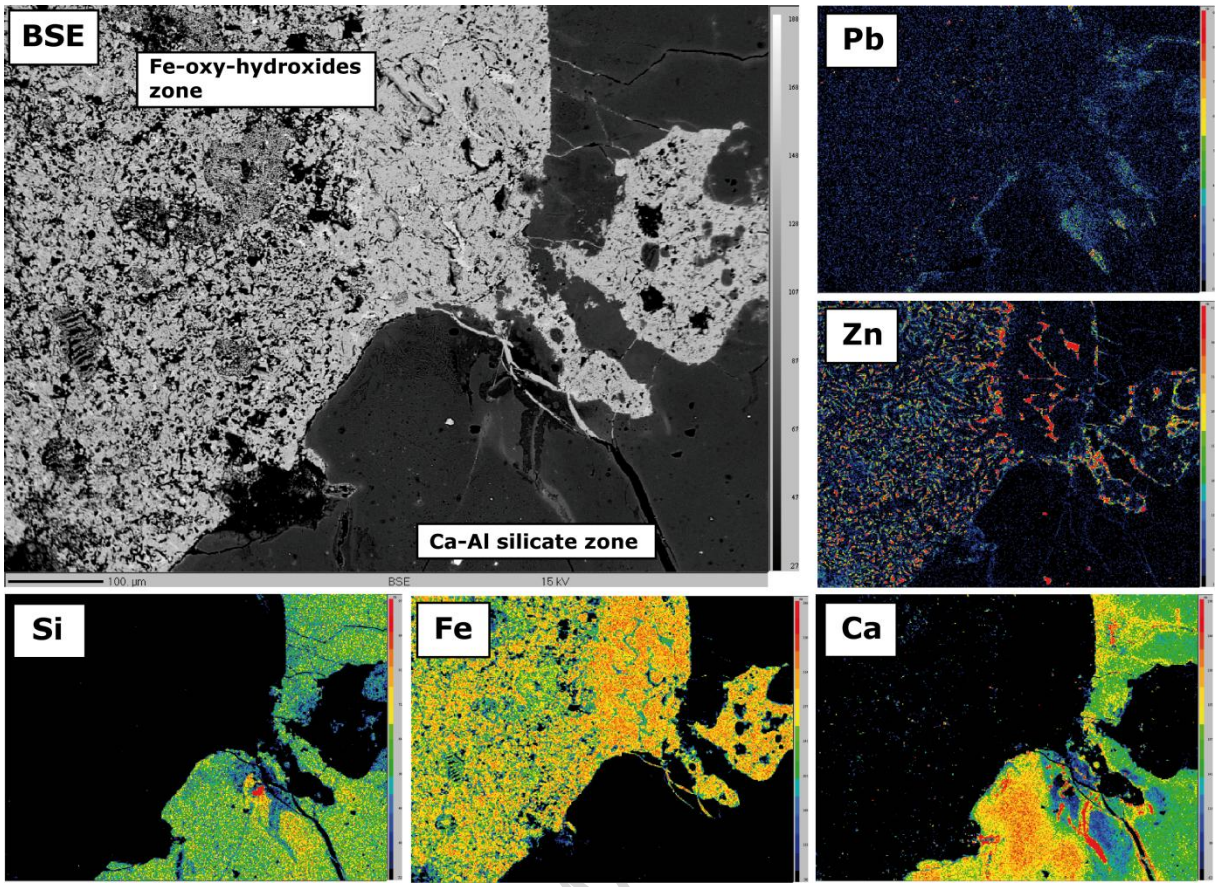

Fig. 4

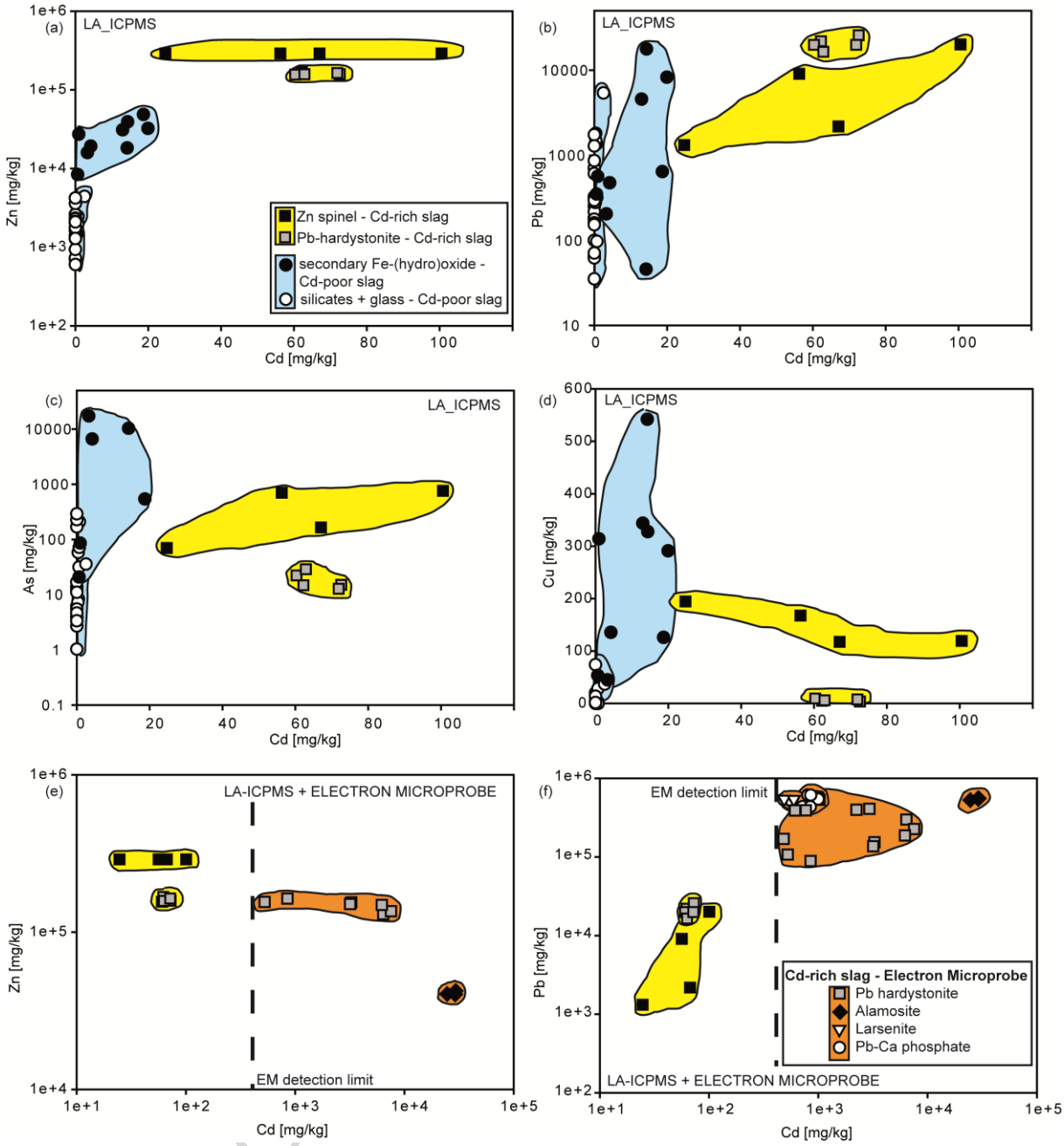

Fig. 5

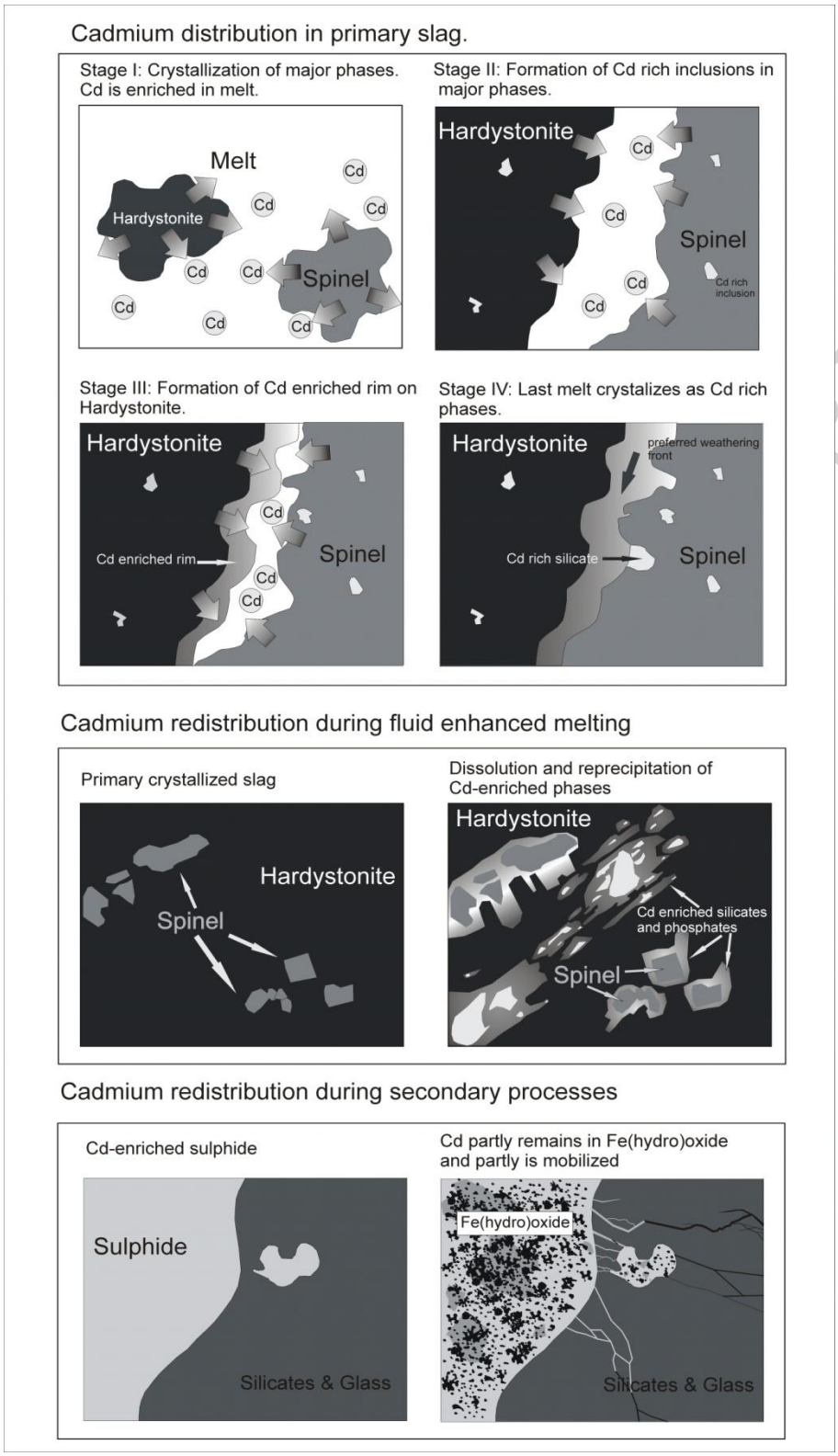

Fig. 6

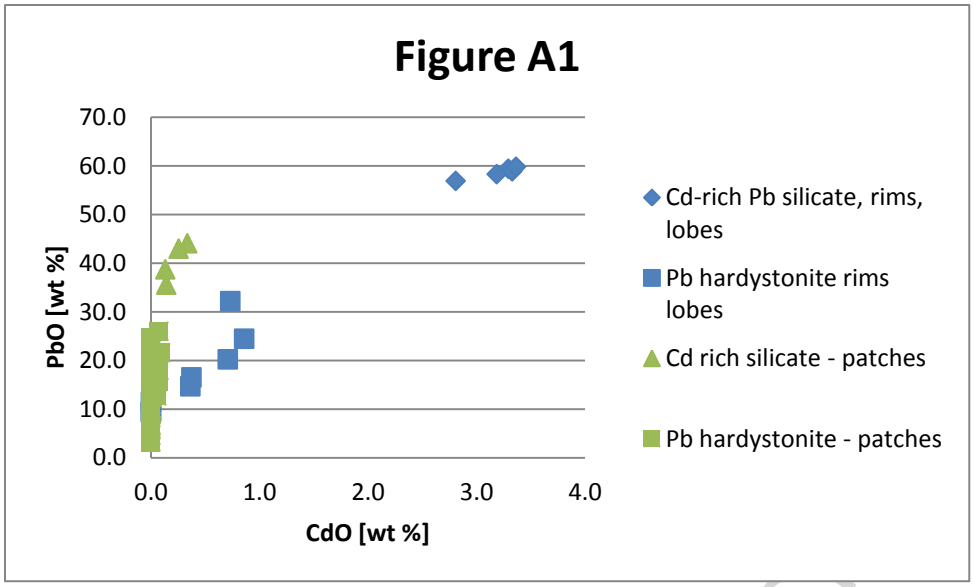

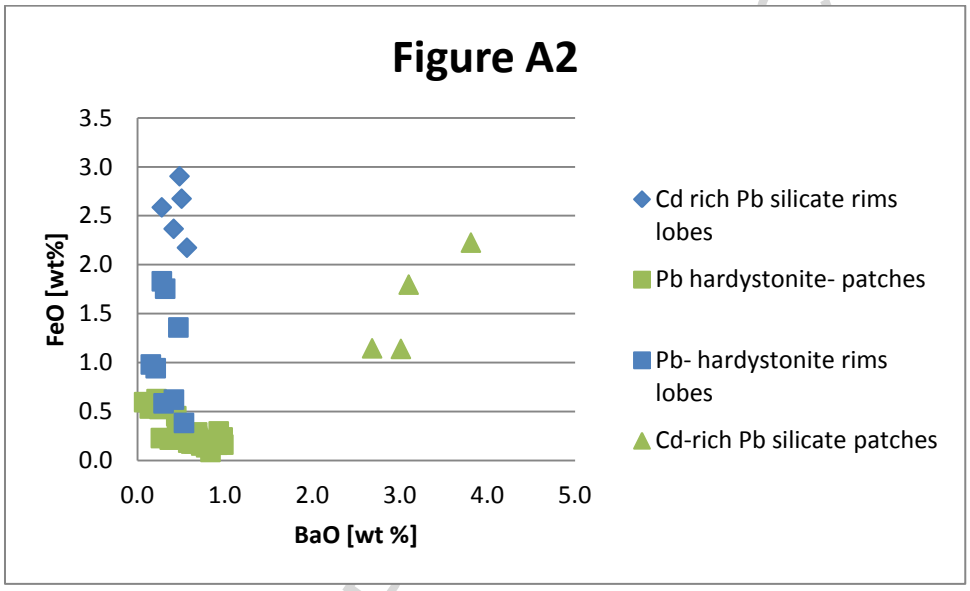

Figure A1, A2: Comparison of Cd, Pb, Ba, Fe concentrations in slag phases from Cd-rich slag between Cd-enriched phases formed due to crystallization of late melts (blue symbols) and Cd-enriched phases formed due to remelting of slag (green symbols).

Table 1 Comparison of Pb, Zn, Cd and As concentrations as analysed in compositionally similar slag phases by electron microprobe and laser ablation inductively coupled plasma mass spectrometry. Analyses of NIST 614 st

Cd poor slag		**Pb**	**Zn**	**Cd**	**As**
EM	Glass	up to 7100 mg/kg	1850 - 14900 mg/kg	bdl	bdl
LAICPMS		35 - 5410 mg/kg	600 - 4400 mg/kg	up to 2,5 mg/kg	1 -290 mg/kg
EM	Fe(hydro)oxide	up to 32000 mg/kg	up to 14800 mg/kg	bdl	bdl
LAICPMS		46 - 17760 mg/kg	18240 - 48520 mg/kg	0,6-19,9 mg/kg	21-89000 mg/kg
EM	Pb rich inclusion in Fe(hydro)oxide	27,4 wt %	3,5 wt %	bdl	bdl
EM	Silicate-Fe(hydro)oxide mix	up to 6300 mg/kg	1,1 - 8,8 wt %	bdl	bdl
EM	Wurtzite	bdl	24,8 wt %	bdl	bdl
Cd rich slag					
EM	Pb-hardystonite	up to 53 wt %	5,9 - 16,3 wt %	up to 7500 mg/kg	up to 18000 mg/kg
LAICPMS		1,8 - 2,8 wt %	15,8 -20,8 wt %	60 -73 mg/kg	13 -29 mg/kg
EM	Zn-spinel	bdl	28,5 wt %	bdl	bdl
LAICPMS		1320 - 20100 mg/kg	36 wt %	25 -100 mg/kg	70 -760 mg/kg
EM	Cd rich Pb silicate	53 wt %	4 wt %	2,4 wt %	0,4 wt %
EM	Pb rich Zn spinel	0,2 - 5,4 wt %	24 - 28 wt %	bdl	up to 1,0 wt %
EM	Pb-Ca-As phosphate	43 -60 wt %	1,3 -2,2 wt %	bdl	3,6 - 7,4 wt %
EM	Pb-Ca Silicate?	16 - 38 wt %	11 -15 wt %	bdl	bdl
EM	Pb-As apatite	1,1 - 2,0 wt %	1,0 -1,8 wt %	bdl	6,7 -8,8 wt %
NIST 614		**Pb**	**Sr**		
	analysed	2.0 ± 0.2	41.2 ± 1.8		
	certified value	2.32 ± 0.04	45.8 ± 0.1		

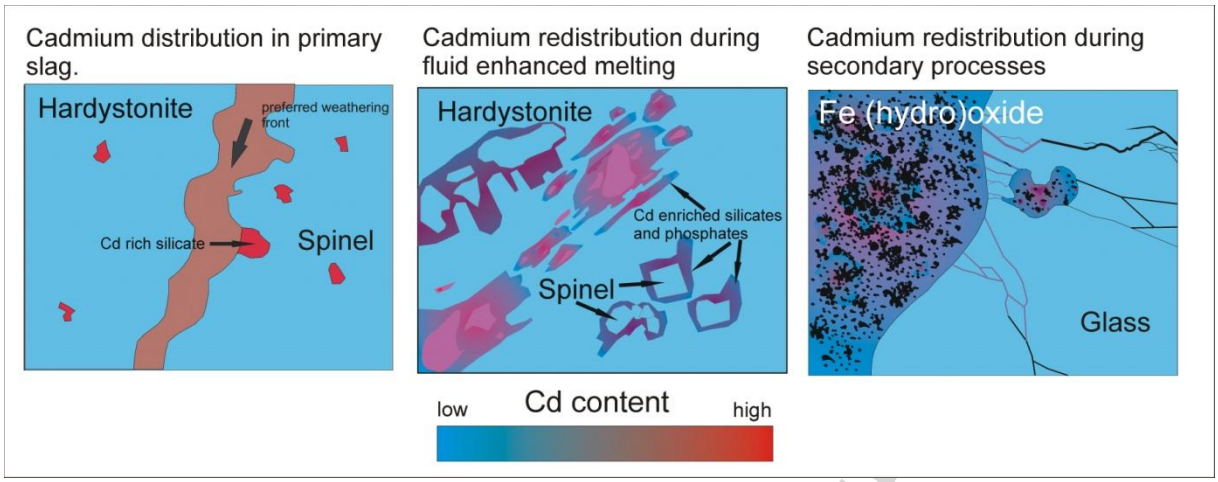

Graphical Abstract

Cadmium distribution in primary slag.

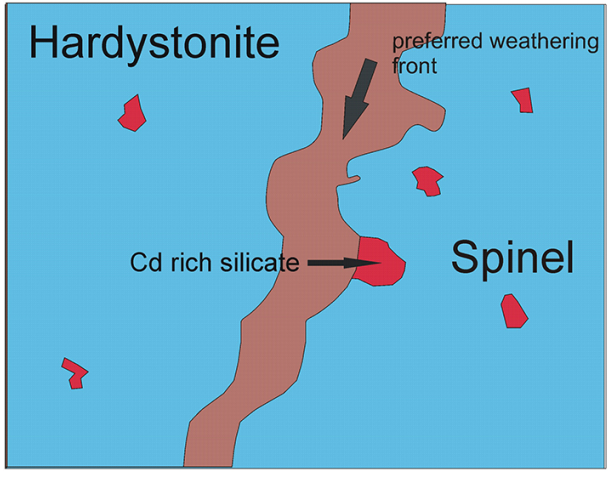

Cadmium redistribution during fluid enhanced melting

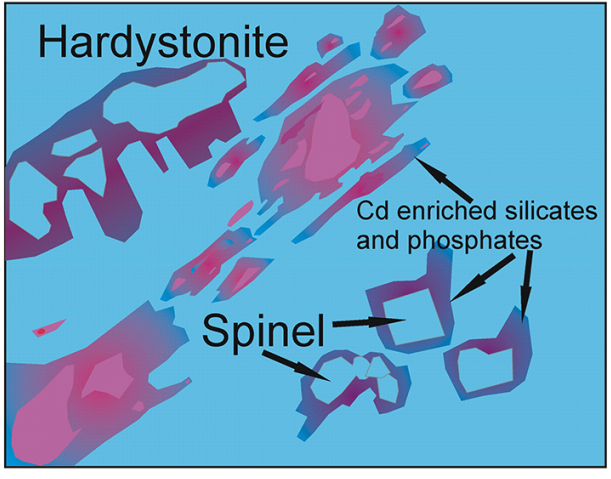

Cadmium redistribution during secondary processes

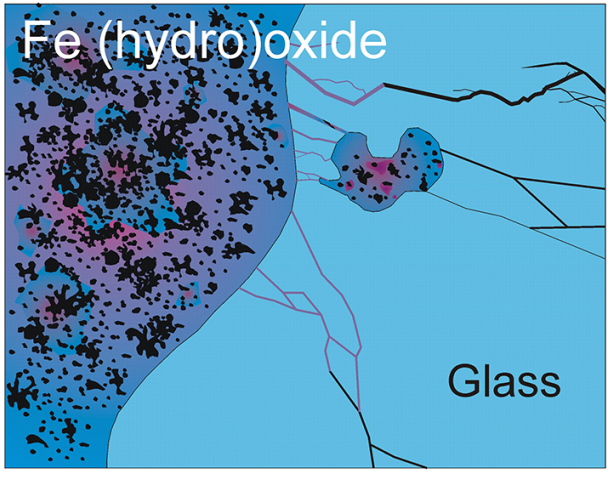

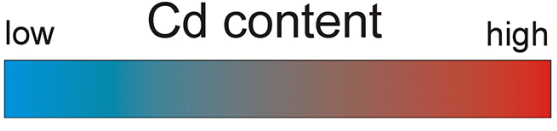

Graphics Abstract

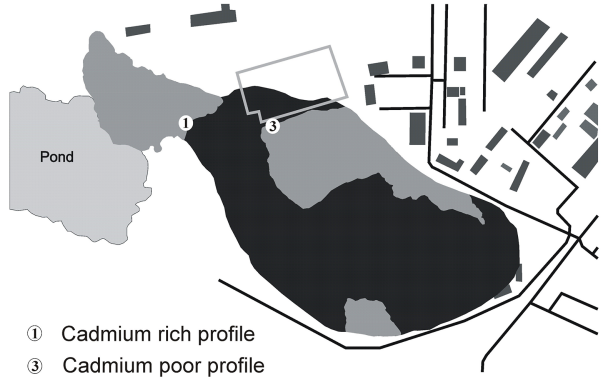

① Cadmium rich profile

③ Cadmium poor profile

Buildings

Slag pile before the removal

Slag pile during the sampling

Roads

Wall

Scale 200 m

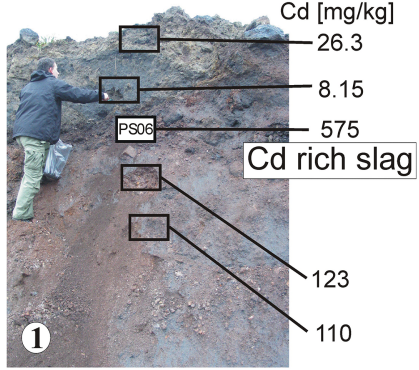

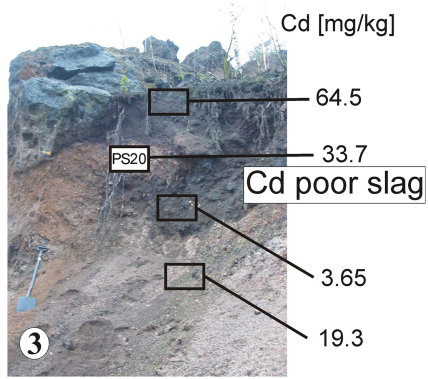

Figure 1

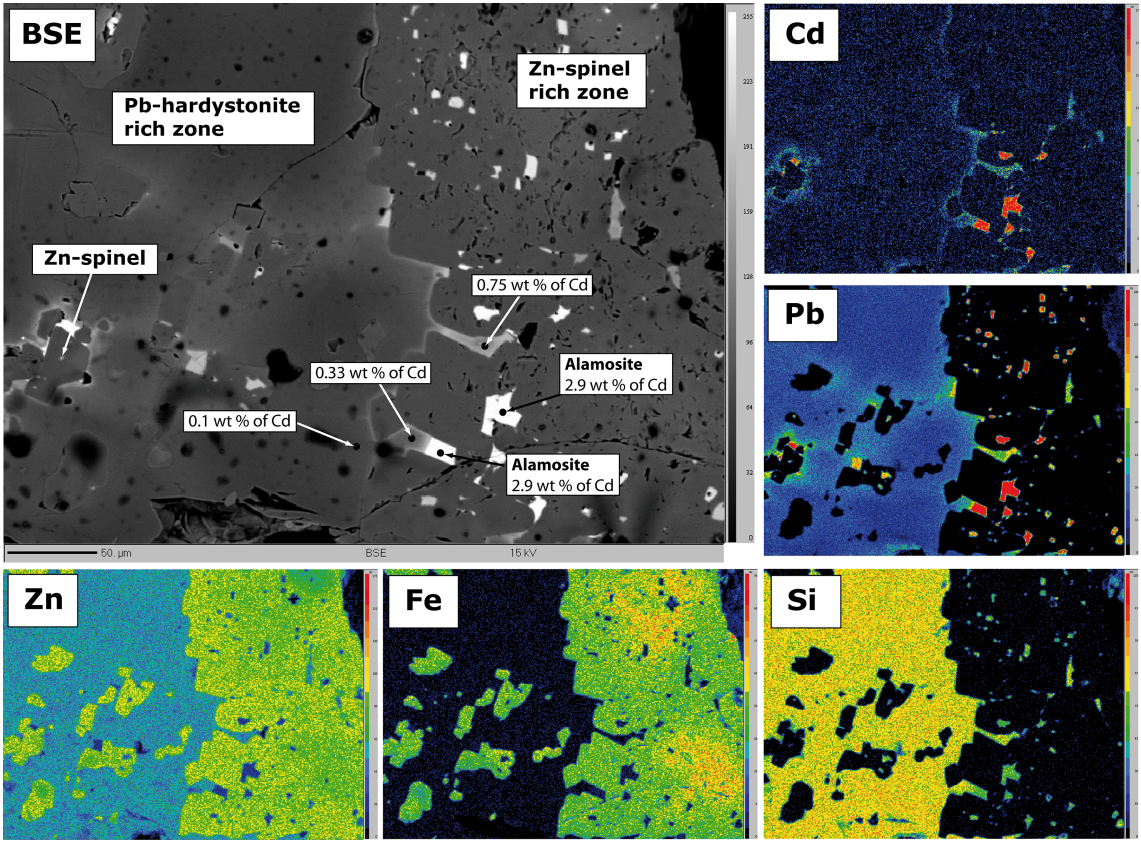
BSE
Pb-hardystonite rich zone
Zn-spinel rich zone
Zn-spinel
0.75 wt % of Cd
0.33 wt % of Cd
0.1 wt % of Cd
Alamosite 2.9 wt % of Cd
Alamosite 2.9 wt % of Cd
50. µm
BSE
15 kV
Cd
Pb
Zn
Fe
Si

Figure 2

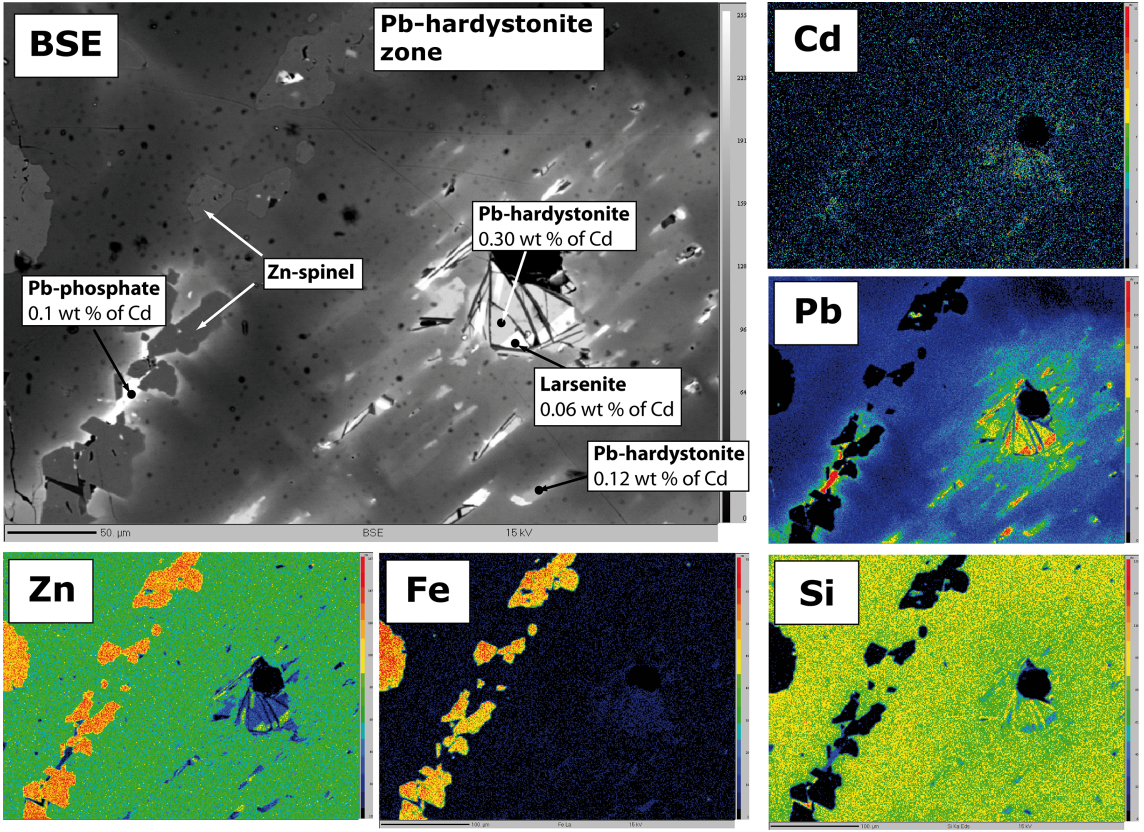
BSE
Pb-hardystonite zone
Pb-hardystonite
0.30 wt % of Cd
Zn-spinel
Pb-phosphate
0.1 wt % of Cd
Larsenite
0.06 wt % of Cd
Pb-hardystonite
0.12 wt % of Cd
50 µm
BSE
15 kV
Cd
Pb
Zn
Fe
Si

Figure 3

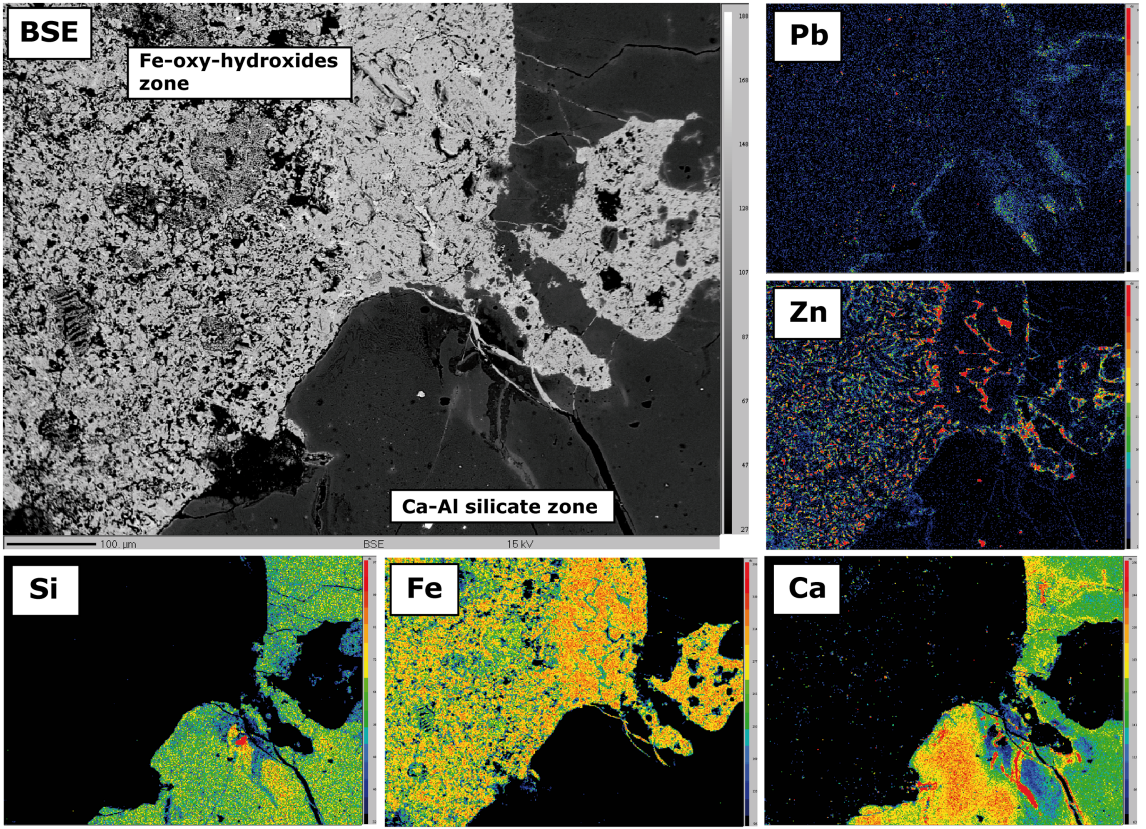
BSE
Fe-oxy-hydroxides zone
Ca-Al silicate zone
100 µm
BSE
15 kV
Pb
Zn
Si
Fe
Ca

Figure 4

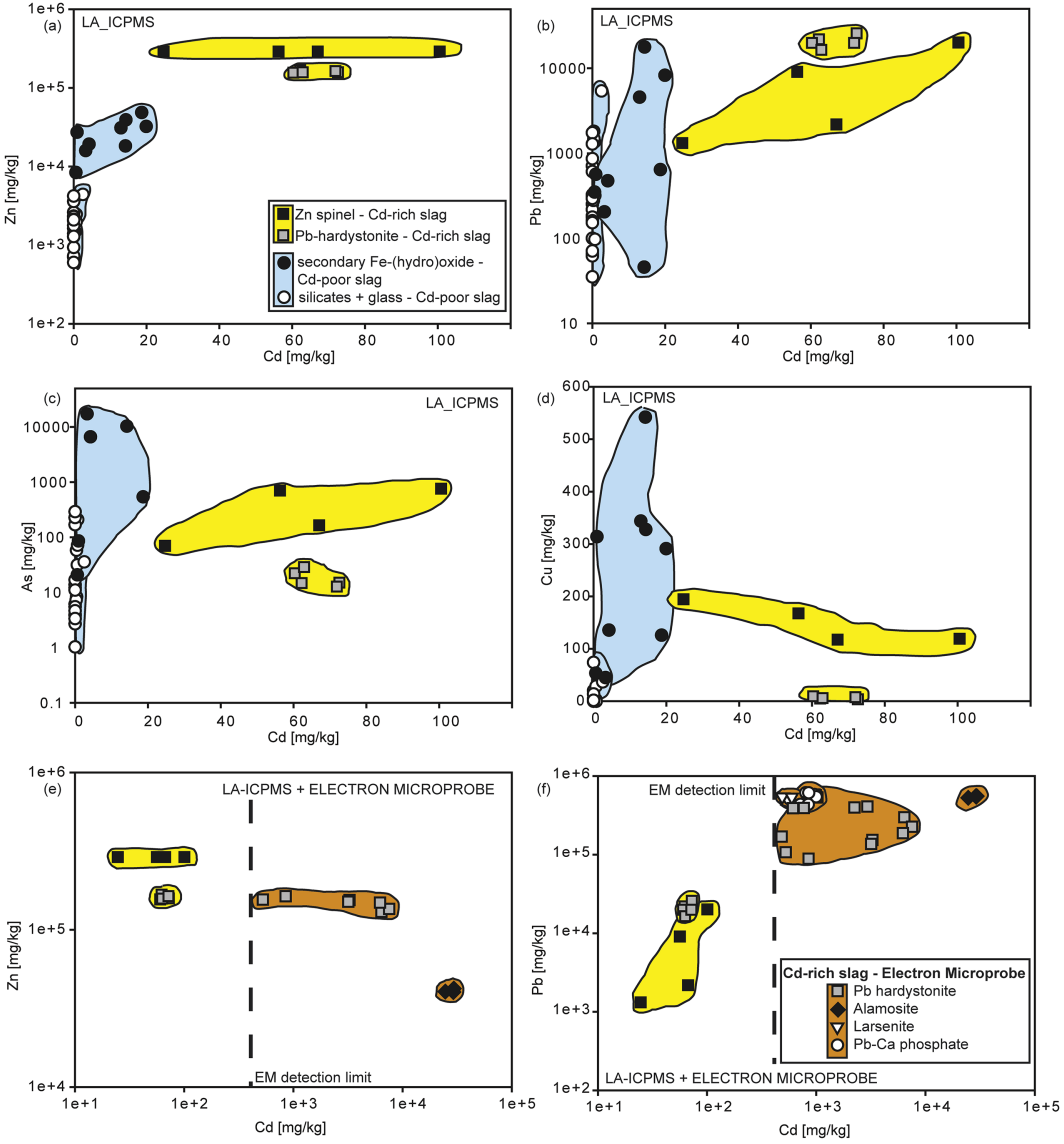
(a)
LA_ICPMS
Zn [mg/kg]
Cd [mg/kg]
Zn spinel - Cd-rich slag
Pb-hardystonite - Cd-rich slag
secondary Fe-(hydro)oxide - Cd-poor slag
silicates + glass - Cd-poor slag
(b)
LA_ICPMS
Pb [mg/kg]
Cd [mg/kg]
(c)
LA_ICPMS
As [mg/kg]
Cd [mg/kg]
(d)
LA_ICPMS
Cu [mg/kg]
Cd [mg/kg]
(e)
LA-ICPMS + ELECTRON MICROPROBE
EM detection limit
Zn [mg/kg]
Cd [mg/kg]
(f)
EM detection limit
Cd-rich slag - Electron Microprobe
Pb hardystonite
Alamosite
Larsenite
Pb-Ca phosphate
LA-ICPMS + ELECTRON MICROPROBE
Pb [mg/kg]
Cd [mg/kg]

Figure 5

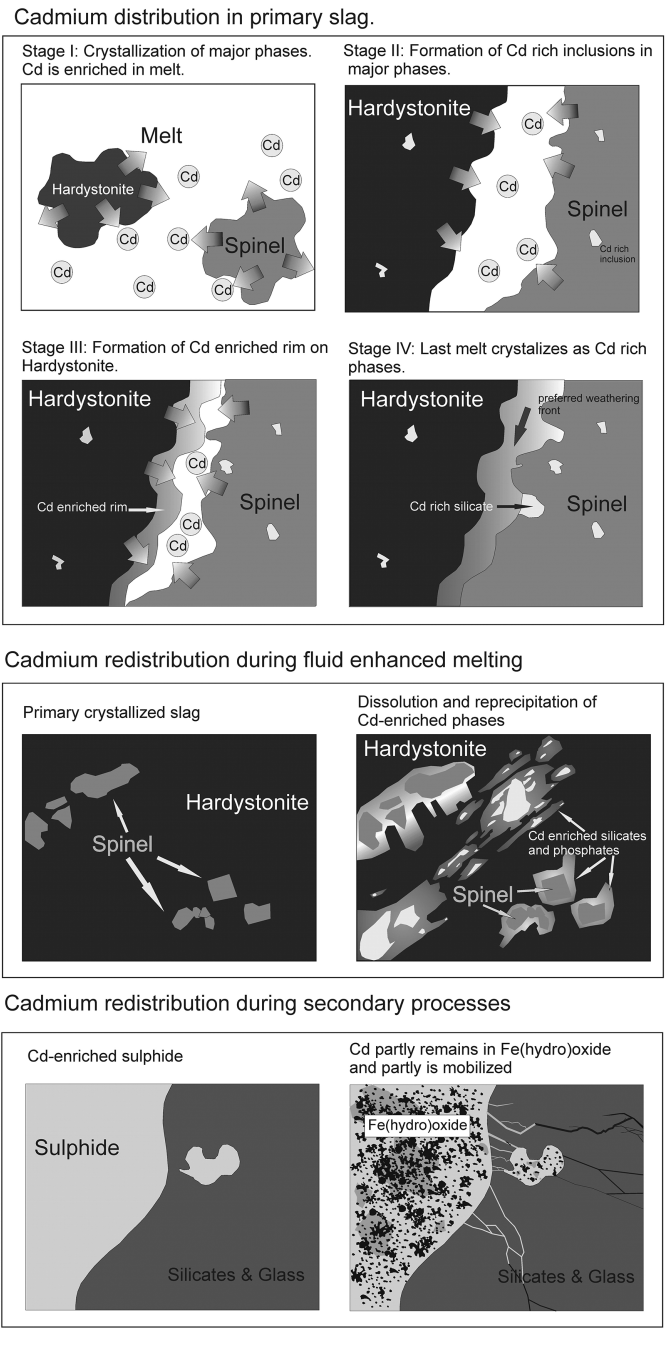
Cadmium distribution in primary slag.
Stage I: Crystallization of major phases. Cd is enriched in melt.
Melt
Hardystonite
Spinel
Cd
Stage II: Formation of Cd rich inclusions in major phases.
Hardystonite
Spinel
Cd rich inclusion
Stage III: Formation of Cd enriched rim on Hardystonite.
Hardystonite
Cd enriched rim
Spinel
Stage IV: Last melt crystalizes as Cd rich phases.
Hardystonite
preferred weathering front
Cd rich silicate
Spinel
Cadmium redistribution during fluid enhanced melting
Primary crystallized slag
Hardystonite
Spinel
Dissolution and reprecipitation of Cd-enriched phases
Hardystonite
Cd enriched silicates and phosphates
Spinel
Cadmium redistribution during secondary processes
Cd-enriched sulphide
Sulphide
Silicates & Glass
Cd partly remains in Fe(hydro)oxide and partly is mobilized
Fe(hydro)oxide
Silicates & Glass

Figure 6